Inexpensive Interferometer for Low Frequency Radio Astronomy

Guilherme S. Rosa, Nelson J. Schuch, Natanael R. Gomes, José R. Bergmann, Ezequiel Echer, and Renato Machado

***Abstract*—An interferometric array similar to the low frequency array (LOFAR) prototype station (LOPES) and to the eight-meter-wavelength transient array (ETA) is being developed to cover the LOFAR frequency range under 100 MHz at the Southern Space Observatory (SSO) (29.4° S, 53.8° W, 480 m. a. s. l.), in São Martinho da Serra, RS, Brazil. In accordance with previous observational spectrum results, the SSO site was classified as being suitable to receive sensitive and sophisticated radio interferometers, based on the phased array concept, similar to those employed at the European LOFAR stations. This paper describes the technical details of development and implementation of a low cost elementary radio astronomy interferometer for the frequency range of 20–80 MHz.**

***Index Terms*—Radio astronomy, antenna arrays, interferometers, circuit noise.**

I. Introduction

LOFAR is a next-generation radio telescope under construction in the Netherlands with long-baseline stations under development in other European countries. LOFAR is an emerging European sensor network with continental dimensions for space and Earth observations. The LOFAR telescope uses phased antenna arrays to form an aperture synthesis telescope for receiving radio signals in the frequency band of 30–240 MHz [1], [2].

There are currently discussions with research institutions from Germany, UK, Italy, France, Poland and Sweden, aiming the installation of LOFAR stations in these countries [1], [2]. These partnerships will extend the "wide area sensor network" and the resolution and sensitivity of the LOFAR system in Europe. The LOFAR telescope will operate in the 30–80 MHz and 120–240 MHz bands (80–120 MHz being dominated by FM radio broadcasting transmissions). As a predecessor to the square kilometer array (SKA) planned to be constructed after 2015, it has a broad impact on the future of Radio Astronomy and Astrophysics, which goes well beyond the current project [1].

To verify whether or not radio emission from cosmic rays is indeed detectable and useful in a modern cosmic ray experiment, Falcke *et al.* [3] built the LOPES experiment. LOPES is a phased array of dipole antennas with digital electronics developed to test same aspects of the LOFAR concept. Considering LOPES, radio emission from cosmic ray air showers at 43–73 MHz on a regular basis with unsurpassed spatial and temporal resolution can be detected [3].

ETA is a new radio telescope consisting of 12 dual polarized 38 MHz resonant dipole elements [4]. ETA has an array of inverted V-shaped design combined with a simple active balun that cover the range of 27–49 MHz [4]. The radio interferometers LOFAR and ETA have used an array of active antennas to achieve the Galactic noise limited operation.

The proposed interferometer is similar to LOPES and ETA methodology. The interferometer proposed in this paper uses simple dipole in conjunction with a preamplifier to operate in the frequency range of ETA, detecting the galactic noise at low frequencies. The ubiquitous galactic synchrotron emission is very strong and can easily be the dominant source of noise in the observation at sub 100 MHz frequency range. Then, the sensitivity of a telescope is limited by galactic noise.

The main objective of the proposed interferometer is the development of a low cost instrumentation compatible with the LOFAR methodologies. The rest of this paper is organized as follows. Section II details the interferometer design. Section III discusses the improvements of the interferometer. Concluding remarks are presented in Section IV.

II. Interferometer

The low cost prototype interferometer proposed here can be generically divided into three components: active antenna, analog receiver and digital correlator. This paper does not discuss about the digital correlator, only the first two components are proposed here.

The active antenna is composed of a dipole radiator, a pair of amplifiers and a balun (see Fig. 1). The amplifier is connected directly to the terminals of the dipole antenna and has as purposes: 1) set the noise temperature of the system, and 2) buffer the impedance between dipole antenna and feedline. Since the employed dipole antenna is balanced [5] and the coaxial cable feedlines are unbalanced, a balun is necessary to transform a balanced line, at the output of the amplifiers, to an unbalanced line at the coaxial cable.

The proposed interferometer employs two super-regenerative receivers deployed for low frequency radio

G. S. Rosa and N. J. Schuch are with the Southern Regional Space Research Center (INPE-MCT) in collaboration with the Santa Maria Space Science Laboratory (LACESM/CT/UFSM), Santa Maria, RS 97105-900, Brazil. E-mail: guilhermeSimonDaRosa@gmail.com and njschuch@lacesm.ufsm.br, respectively. N. R. Gomes and R. Machado are with the Department of Electronics and Computing, Federal University of Santa Maria and Santa Maria Space Science Laboratory, Technology Center (CT/UFSM), Santa Maria, RS 97105-900, Brazil. E-mail: natanael.rgomes@gmail.com and renatomachado@ieee.org, respectively. J. R. Bergmann is with the Center for Telecommunications Studies, Catholic University of Rio de Janeiro (CETUC/PUC-Rio), Rio de Janeiro, RJ 22453-900, Brazil. E-mail: bergmann@cetuc.puc-rio.br. E. Echer is with the Division of Space Geophysics, National Institute for Space Research (DGE/CEA/INPE-MCT), São José dos Campos, SP 12227-010, Brazil. E-mail: eecher@dge.inpe.br.

This paper was presented in part at the International Information and Telecommunication Technologies Symposium (I2TS'2010), Rio de Janeiro, Brazil, December 2010.

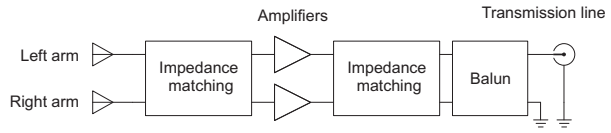

Fig. 1. Basic concept for a low frequency radio astronomy active antenna of LOFAR.

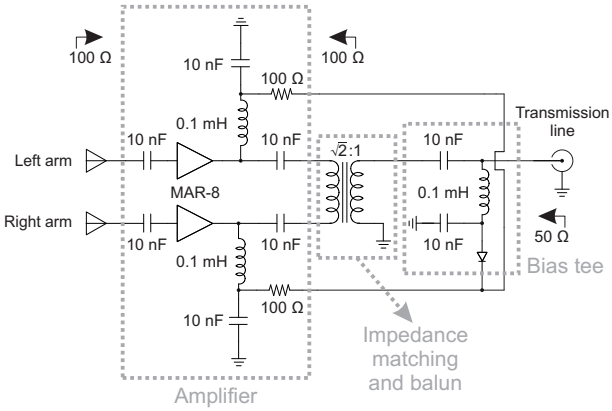

Fig. 2. The complete active antenna circuit.

astronomy applications. According to [6], the super-regenerative receiver has a reduced cost and a low power consumption. The receiver prototype is a hybrid model of software-defined radio (SDR), because its output signal is at audio frequency, and also due the interferometer correlation is performed by software.

Next, we present in more details the components of the implemented prototype.

A. Active Antenna

The configuration of LOFAR active antennas [2] is shown in Fig. 1. An impedance transformer network provides the impedance matching between the dipole and the amplifiers. At the output of the amplifiers there are two more transformers: one determines the impedance of the transmission line and the other transformer unbalances the signal, coming from the center dipole, for transmission into a coaxial cable RG-213 (50 Ω). Fig. 2 shows a transformer with voltage transformation ratio of $\sqrt{2}$:1 in order to match the impedance between the output of the amplifiers and the coaxial cable input.

The configuration of the active antenna implemented in the proposed interferometer follows the precepts of the radio telescope ETA [4]. In this configuration, the use of separate amplifiers reduces significantly the common mode current that could occur if the dipole is directly connected to the transformer [7]. The amplifier circuit of the prototype uses two Mini-Circuits MAR-8 monolithic amplifiers that offer [8] high gain, input and output impedances of 50 Ω, and low noise figure. The complete circuit of the active antenna is shown in Fig. 2.

The power of the amplifiers is performed through a bias tee circuit. Thus, in the coaxial cable exists a direct current (DC) signal – inserted into the receiver – and a radio frequency (RF) signal – that is provided by the balun output. At the receiver there is a bias tee identical in order to filter DC and RF signals.

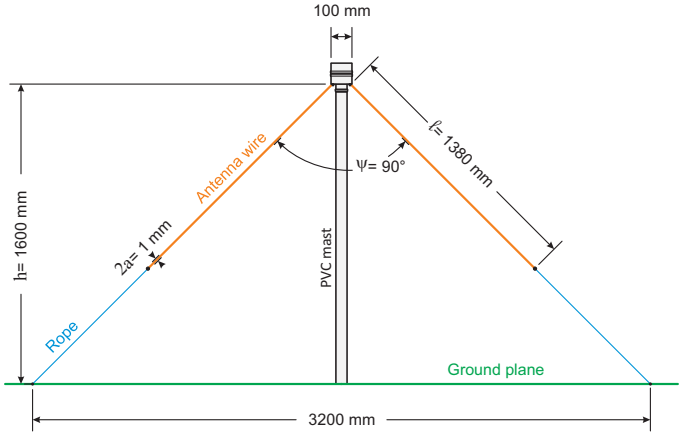

Fig. 3. A LOFAR LBA like, proposed in [9].

The LOFAR low band antenna (LBA) frequency range is from about 10 MHz (near the ionosphere cut-off frequency) to 80 MHz [9]. To operate successfully in this frequency range an inverted V dipole antenna is used with a ground plane reflector, as shown in Fig. 3, and resonance frequency around 51.5 MHz [9].

For the proposed interferometer, a simple inverted V-shape dipole was constructed with 1 mm copper wire. This antenna was analyzed using NEC-2 based method of moments (MM) and using finite element method (FEM) employed by HFSS software. The ground scenario considered was realistic lossy ground having conductivity of $\sigma = 5 \times 10^{-3}$ S/m and relative permittivity $\varepsilon_r = 13$.

The simulation results of impedance and standing wave ratio (VSWR) for the dipole antenna using a realistic ground are presented in Fig. 4 and Fig. 5. The standing wave ratio is normalized to the preamplifier input impedance, which is of 100 Ω, (2 MAR-8 @ 50 Ω = 100 Ω). We can see that the minimum VSWR (VSWR = 2) occurs for the resonance frequency (∼51.5 MHz). In other words, it means that at this frequency the antenna impedance is 50 Ω (essentially a real value). It shows a very good agreement with results of [10], who studied this type of antenna.

1) Galactic Noise Model: The usable bandwidth of the active antenna is one in which the galactic noise dominates the instrumentation noise. The model proposed by Cane [11] for the galactic noise background was employed to evaluate the usable galactic noise limited bandwidth. The galactic noise power can be described in terms of the intensity I_ν integrated over the antenna pattern. An approximation for I_ν can be obtained from [11], which quantified the spectrum of the galactic noise background based on observations of the Galaxy polar regions at four frequencies between 5.2 and 23.0 MHz. From these measurements, it was determined that the intensity is given in units of W m^{-2} Hz^{-1} sr^{-1} by

$$I_\nu = I_g \nu^{-0.52} \frac{1 - e^{-\tau(\nu)}}{\tau(\nu)} + I_{eg} \nu^{-0.80} e^{-\tau(\nu)}, \qquad (1)$$

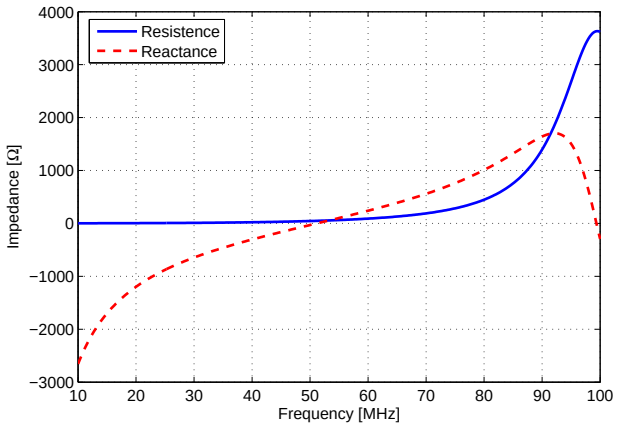

Fig. 4. NEC-2 simulated impedance for the antenna shown in Fig. 3 using a realistic ground.

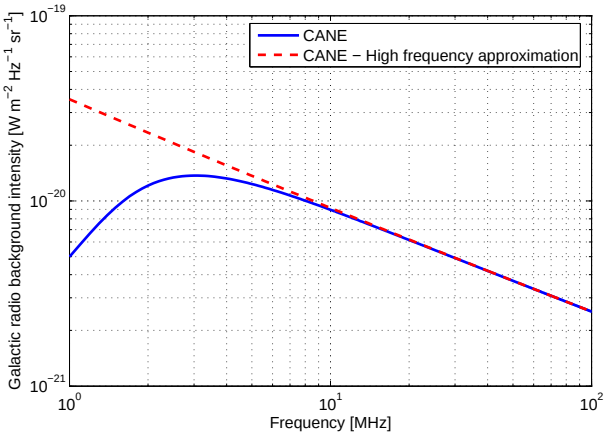

Fig. 6. Galactic noise intensity. Solid blue line: Cane model. Dashed red line: approximation of Cane for high frequencies.

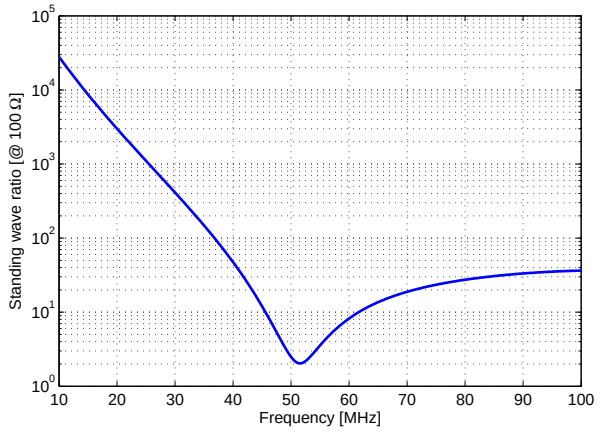

Fig. 5. NEC-2 simulated standing wave ratio for the antenna shown in Fig. 3 using a realistic ground.

where $I_g = 2.48 \times 10^{-20}$, $I_{eg} = 1.06 \times 10^{-20}$, $\tau(\nu) = 5.0\,\nu^{-2.1}$, and for this case, ν is frequency in MHz. I_g and I_{eg} are the coefficients obtained by Cane in [11], and this result has been successfully used to calibrate telescopic observations of great field vision [5]. The above expression is given in units of steradian (sr), i.e., measures of the current on a solid angle.

In (1), the first term applies to the contribution of the galaxy itself, whereas the second term is due to extragalactic noise, which is assumed to be spatially uniform.

A good approximation to (1) for the spectrum above 10 MHz is given by

$$I_\nu \approx I_g \nu^{-0.52} + I_{eg} \nu^{-0.80}. \tag{2}$$

The Cane high frequency galactic noise model, given by (2), is used throughout this paper. Thus, the performance of antennas is underestimated[1]. Equations (1) and (2) are represented as a function of frequency in Fig. 6.

The result in (2) applies to the Galaxy poles since the noise intensity is correlated with the mass distribution in the Galaxy, a result which represents a minimum range, while the noise in the direction of the galactic plane is somewhat larger. However, as the galactic plane remains spatially unresolved at low gain antennas, the additional contribution of noise is relatively small [5].

2) Active Antenna Bandwidth Evaluation: The main requirement of the active antenna system is that it provides a signal to the receiver where the dominant noise is the unavoidable galactic noise.

The determination of the degree to which the receiver input is limited by the galactic noise requires knowledge of the noise temperature system contributions. From Friis formula for cascaded of two-ports, considering the situation of active antenna shown in Fig. 1 followed by a receiver, the system noise temperature is given by

$$T_{sys} = T_{sky} + T_a + \frac{T_r}{G_a}, \tag{3}$$

where the T_{sky} is defined to be the antenna equivalent temperature corresponding galactic noise, the T_a is the active antenna noise temperature, G_a is the gain of active antenna and the receiver noise temperature is T_r.

The value of T_{sky} is diagrammed in Fig. 7, using the Cane approximation for high frequency. Fig. 7 highlights the antenna temperature of the extremes frequency of interest. At 20 MHz the antenna temperature is about 50000 K and at 80 MHz it is about 1500 K. Thus, the noise temperature of the whole active antenna cannot exceed 1500 K at 80 MHz.

Due to the MAR-8 amplifier gain, which is about 30 dB [8], G_a is sufficiently large for allowing T_r to be neglected. Since, according to [5], the ground noise can be neglected, and the man-made noise, which is characterized in [12] is also neglected, the active antenna system was modeled considering the galactic noise and the instrumental noise. The instrumental noise is formed by the noise temperature contribution of preamplifier and the transmission line.

The contribution of temperature due to the galactic noise is the power spectral delivered to the receiver. Let S be the power spectral density of the signal associated with T_{sky} at the output of feedline. Given the Cane galactic model for the

[1]As we can see from Fig. 6, Equation (2) overestimates the noise at the lower frequencies.

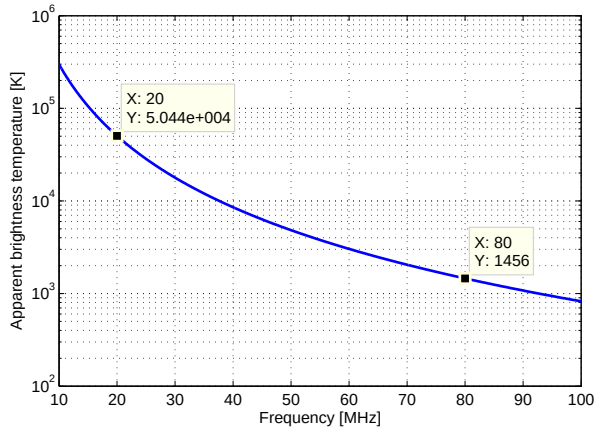

Fig. 7. Antenna brightness temperature received by a low-gain antenna, as a function of frequency using the Cane high frequency galactic noise model.

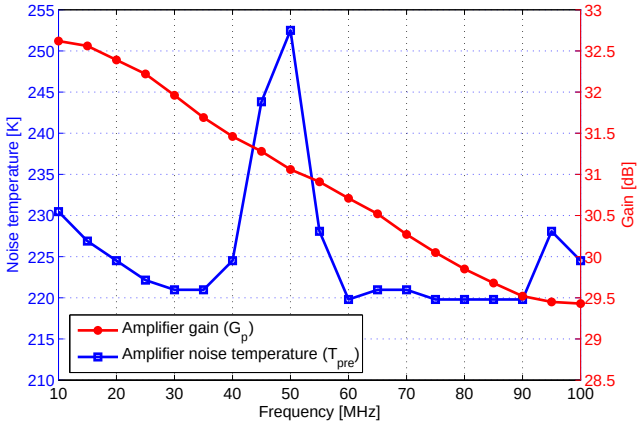

Fig. 8. Measured noise temperature (line with point markers) and gain as a frequency function. The maximum noise temperature (line with square markers) is 252.5 K.

system, S becomes

$$S = e_r k T_{sky}(1 - |\Gamma|^2) G_p G_f, \tag{4}$$

where G_p is the preamplifier gain, G_f is the feedline gain, and $(1 - |\Gamma|^2)$ represents the fraction of power available at the antenna which is successfully transferred to the preamplifier. This fraction is nominally 1, but is often much smaller than one due to impedance mismatch between the antenna and amplifier. Γ is the voltage reflection coefficient on the antenna terminals looking into the preamplifier and is given by

$$\Gamma = \frac{Z_p - Z_a}{Z_p + Z_a}. \tag{5}$$

The preamplifier noise as measured at the input of receiver can be defined in terms of the preamplifier input-referenced noise temperature T_{pre} as

$$N_p = k T_{pre} G_p G_f. \tag{6}$$

Finally, the noise resulting from the transmission line loss can be significant. The noise at the end of the feedline can be described in terms of the physical temperature T_{phys} as

$$N_f = k T_{phys}(1 - G_f). \tag{7}$$

The ratio γ of galactic noise to instrumental noise measured at receiver input is given by

$$\gamma = \frac{S}{N_p + N_f}. \tag{8}$$

The noise temperature and the preamplifier gain was determined by the measurement of the MAR-8, see the measurement results in Fig. 8.

The transmission line considered was a 100 m RG-213 coaxial cable. The operating temperature chosen was T_{phys} = 290 K (∼20 °C) with a gain associated with the transmission line (coaxial cable RG-213) ranging from -2 dB to -6.9 dB, between 10 and 100 MHz, respectively.

The comparison between the instrumentation active antenna noise (feedline and preamplifier) and the galactic noise is shown in Fig. 9. The antenna efficiency is considered unitary

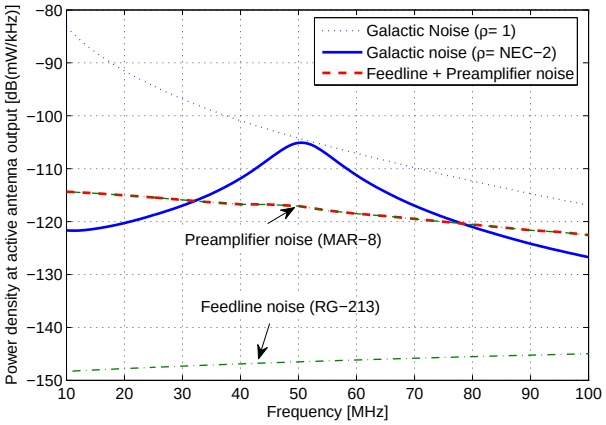

Fig. 9. Comparison between the instrumental active antenna noise (dashed-strong red) and the galactic noise (solid-strong blue). The noise due to a system with standing wave ratio equal to 1 (perfect impedance matching) is represented by the dashed line.

for the entire paper, which is a good assumption for copper wire antennas. According to Fig. 9, we can conclude that the active antenna operates limited by the galactic noise in the frequency range about 32.1–78.2 MHz, which does not meet the requirement of the interferometer. Further analysis will be done about this limitation in Section III.

B. Analog Receiver

The new generation of radio telescopes like the LOFAR, long wavelength array (LWA) and SKA is composed by thousands of antennas spread over stations (which are formed by tens of antennas) that cover continental extensions [5], [13]. The amount of receptors is directly proportional to the number of antennas. Therefore, it is evident the interest in reducing the cost of RF receivers used in large radio telescope.

The use of classic RF receivers, such as the superheterodyne receiver topology, results in high costs for large interferometers. The frequency range of the receiver described here is 20–80 MHz. The proposed receiver employs the super-

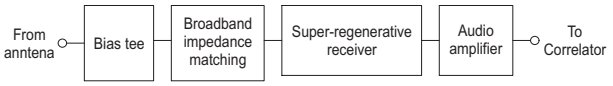

Fig. 10. Receiver topology.

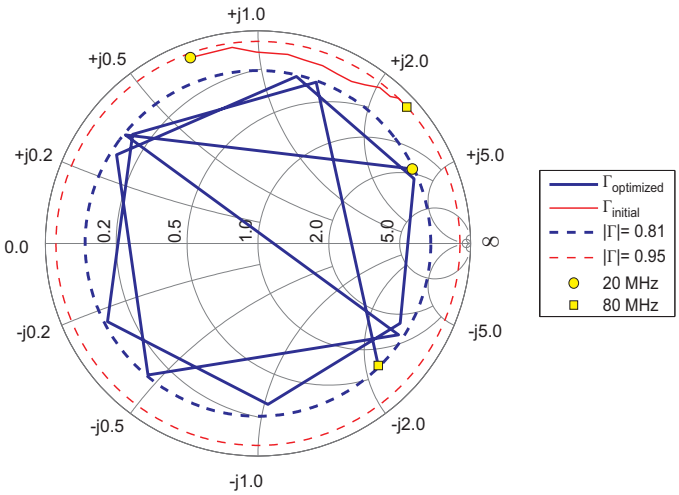

Fig. 11. Reflection coefficient measured (solid red) without the impedance matching network; reflection coefficient using the impedance matching network (solid-strong blue), the maximum value of the reflection coefficient modulus measured (dashed red) and maximum reflection coefficient modulus of the optimized network (dashed-strong blue). The reflection coefficients are normalized to 50 Ω.

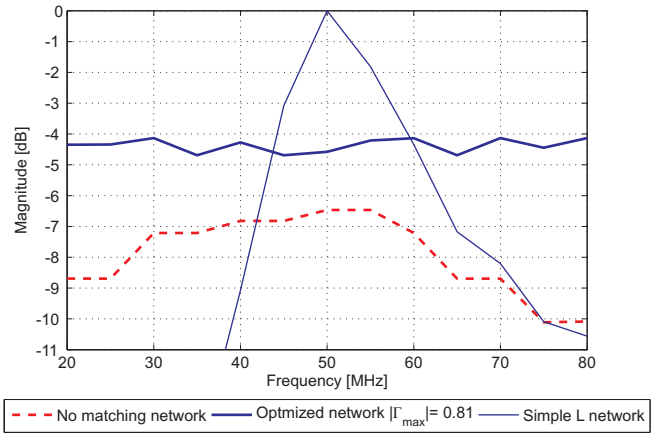

Fig. 12. Frequency response of the magnitude of power delivered to the receiver input: 1) without the impedance matching network (dashed red), 2) using the optimized impedance matching network (solid-strong blue) and 3) using a single L network (solid blue).

regenerative topology motivated primarily by the low cost of this type of receiver.

In order to overcome the major problems present in the super-regenerative receiver architecture [14], it was proposed a receiver topology composed by: 1) a bias tee, 2) an impedance matching network for 20–80 MHz, 3) a super-regenerative receiver, and 4) an audio amplifier stage, as shown in the block diagram of Fig. 10.

Bias tee block is used to feed the active antenna amplifiers and its design and operation details are shown in [15], [16], moreover, their components are equal to the bias tee located in active antenna. It is important to mention that the employed bias tee does not insert significant noise in the RF signal and does not significantly alter the impedance of receiver input. Therefore, the electrical analysis of bias tee circuit can be overlooked.

The impedance matching network for 20–80 MHz was designed from impedance measurements at the receiver input. Fig. 11 shows the initial values of the reflection coefficient $\Gamma_{initial}$ (normalized to 50 Ω) measured as a function of frequency. It can see that the characteristic of the reflection coefficient, and consequently the receiver impedance input is highly nonlinear and presents very high values, with a maximum of 0.95 for Γ.

The possibility of using classical techniques of impedance matching, either with network L, Pi or T [15], [16] was discarded. According to [16], Pi and T networks are extremely narrow-band and L network is best suited for smaller values of quality factor Q, which is inversely proportional to bandwidth. Reference [16] affirms that the cascading of multiple networks L, following several design parameters, can minimize the Q factor of a network. However, despite increasing the bandwidth, this technique has some weaknesses: the impedance matching will always be optimized to a center frequency design and the signal will be degraded in the periphery of the central frequency. Tens of cascaded L networks would be required to obtain a impedance matching for a bandwidth of 60 MHz (20–80 MHz) and the values for the network components can be impracticable as the number of cascaded networks increase very much.

Furthermore, in case of the proposed receiver, the design of multiple cascaded L networks would be designed to the impedance at center frequency (50 MHz), ignoring the large variations of receiver input impedance, as shown in Fig. 11.

The frequency response of the impedance matching of a simple L network is shown in Fig. 12, and it is evident that this impedance matching technique is not applicable to the receiver proposed here. The impedance matching network was designed from the input impedance measurements in the super-regenerative receiver block.

An iterative algorithm was implemented to minimize the module of reflection coefficient $\Gamma_{initial}$ measured at the receiver input from the insertion of an LC network: a 5^{th} order bandpass filter was chosen for the filter network.

On the algorithm, a function F(L,C) calculates the reflection coefficient based on the values of L and C of the filter and based on the values of measured receiver impedance. The result of this function is the sum of the reflection coefficients for frequencies between 20–80 MHz. The frequencies assessed are those where the values of $\Gamma_{initial}$ were measured.

The operation of the algorithm is as follows: from the initial values of L and C, the reflection coefficient seen by the receiver input is calculated. In the first step of optimization, all values of L and C are varied. When a local minimum of F is found, the values of L and C of the optimized network are stored. However, these values of capacitances and inductances are not values commercially encountered. Therefore, in the next step, all values of C are approximated by commercial

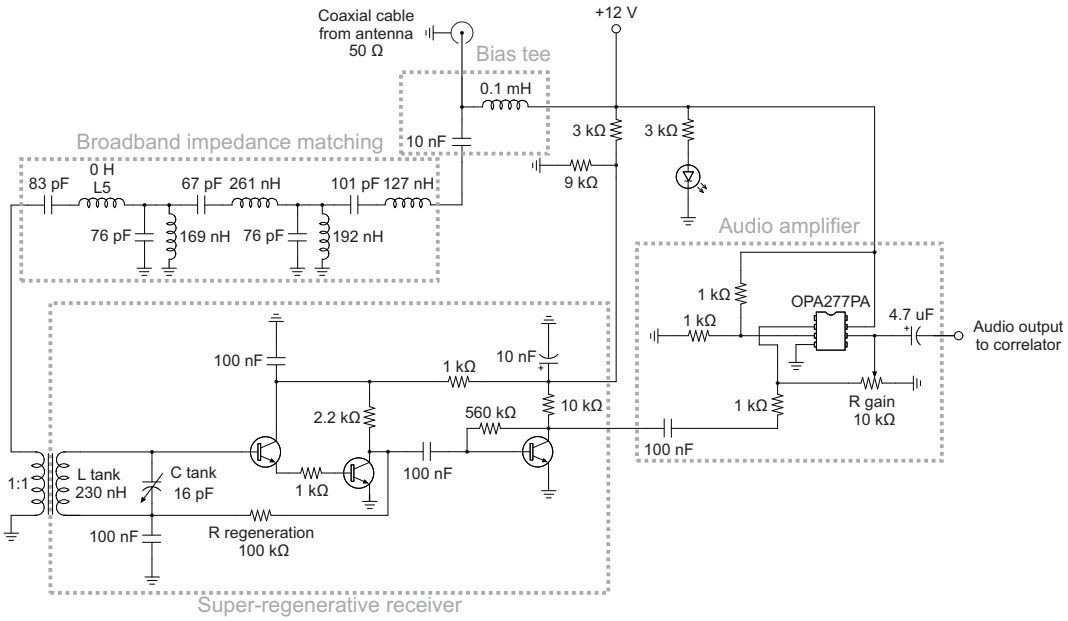

Fig. 13. Complete analog receiver circuit.

values.

In the third step, the optimization is performed once again, but now only on the values of L. When a local minimum of F is found, one of the values of the inductors is approximated by an inductance available (i.e. an inductance value of an inductor that was constructed and measured). In the next step, the selected inductor gets out of the free variables of optimization. At this point there are only four inductors to be optimized. Then, the optimization is performed again, but now only over the four remaining L values. When a local minimum of F is found, one of the values of the inductors is approximated by an available inductance. The process repeats until all inductors are optimized.

The impedance response results using the optimized matching network are shown in Fig. 11. The broadband impedance matching network circuit is shown in Fig. 13, along with the full proposed receiver circuit.

From the results shown in Fig. 12, it can be observed the occurrence of a distortion of the frequency response of the Chebyshev filter which served as the initial value for the network elements. The inductor L5, see Fig. 13, was unnecessary: after network optimization the inductor value became nearly zero. The impedance matching components values are shown in detail in Fig. 13.

Through the network impedance matching was possible to limit the attenuation of the initial super-regenerative receiver that had an attenuation exceeding 10 dB with ripple of 3.5 dB to a frequency response with maximum attenuation of 4.5 dB and ripple of 0.5 dB, as shown in Fig. 12.

The super-regenerative receiver considered in the block diagram in Fig. 10 follows the operation line of the circuit integrated (CI) MK484 (see Fig. 14), a high sensitivity amplitude modulation (AM) receiver [17]. However, according to MK484 data sheet [17], this CI has an input operating frequency between 150 kHz–3 MHz Thus, as in the absence of a low-cost CI that operates in the frequency range of interest (20–80 MHz), a receiver was developed with transistor logic using the same MK484 concept. The transistors used in the receiver shown in Fig. 13 are general purpose BC548 NPN transistor, which has a typical operating frequency up to 150 MHz [18].

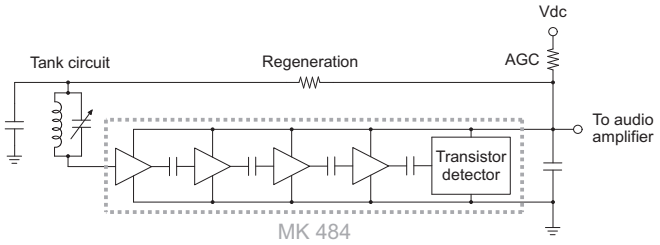

Fig. 14. Basic circuit receiver using the MK484. Adapted from MK484 data sheet [17].

The last step of the basic topology of the receiver is the audio amplifier. This step was performed with an OPA277PA operational amplifier. The CI was fed asymmetrically (to limit the amplifier output voltage to values compatible with the maximum permissible limits of the computer sound card used in correlation data acquisition step). The complete circuit is shown in detail in Fig. 13.

III. Interferometer Improvements

In Section III it is discussed the improvements were made in the active antenna and analog receiver described previously. The main motivation for making this update on the instrumentation was to mitigate the implemented receiver frequency offset and investigate changes in the radiant system in order to increase the active antenna bandwidth galactic noise limited. We aim to lower the interferometer costs with these improvements. In this sense, at the end of Section III, we present a cost analysis of the implemented interferometer taking into account the described improvements.

A. Antenna Investigation

The active antenna operates satisfactorily in the frequency range of 32.1–78.2 MHz, as shown in Fig. 9. However, as we seek to develop a prototype compatible with LOPES, operating between 20 and 80 MHz, the main parameters that can be modified in order to increase usable bandwidth are: 1) noise temperature of the preamplifier, 2) preamplifier input impedance and 3) filamentary antenna changes aiming lowest standing wave ratio between the dipole and preamplifier. The initial two parameters involve changes in the active balun, and *a priori* imply a certain instrumental cost. The optimization of filamentary antenna has negligible cost compared to other parameters: basically involves the shape and size of the antenna. Thus, the improvements are focused in the filamentary antenna.

1) Inverted V Dipole Antenna: According to Fig. 9, the feedline noise can be made negligible compared to the preamplifier noise, since it is visually quite difficult to distinguish the $N_p + N_f$ and N_p curves in figure. Thus, we can simplify (8) to

$$\gamma \approx e_r \frac{T_{sky}}{T_{pre}}[1 - |\Gamma|^2]. \tag{9}$$

The impedance match between antenna and preamplifier is often characterized in terms of the voltage standing wave ratio, defined as

$$\rho = \frac{1 + |\Gamma|}{1 - |\Gamma|}, \tag{10}$$

and therefore (9) can be written as

$$\gamma \approx e_r \frac{T_{sky}}{T_{pre}} \frac{4\rho}{(\rho + 1)^2}. \tag{11}$$

For extremely badly matched antennas, a large value of VSWR simplifies (11) to

$$\gamma \approx e_r \frac{T_{sky}}{T_{pre}} \frac{4}{\rho}. \tag{12}$$

A preliminary analysis of (12) indicated that using an inverted V dipole radiator that have a more favorable impedance matching, i.e., a better VSWR, the active antenna would extend the operating range limited by the galactic noise.

According to [10], who analyzed the V dipole antenna with center feed, this type of antenna can be geometrically characterized by three parameters: 1) the dipole arm length ℓ, 2) radius of the wire dipole a, and 3) the opening angle between the dipole arms Ψ. In the study by [10] it is evident that the dipole impedance does not vary significantly for Ψ between 120° and 180°. With Ψ = 90° the real part of impedance presented lower values compared to those found for larger values of the opening angle between the arms of the dipole. In contrast, there is significant growth of the reactance to Ψ for larger opening angles. Comparisons on the variation of Ψ are verified independently of a and ℓ settings. Overall, it appears that Ψ = 90° presents the figures more favorable to increasing the galactic noise limited bandwidth. Therefore, the investigation will focus only on a and ℓ configurations, and will keep the implemented antenna Ψ = 90°. According to [10], both resistance and reactance of a dipole V fed symmetrically at the center decreased with the reduction of the value of ℓ/a. The first parameter investigated is the conductor diameter $2a$. The simulations shown in Fig. 15 kept the same dimensions of the antenna presented by Fig. 3, except the value of $2a$. The same conditions of instrumental noise used previously (see Fig. 9) were used to calculate the γ curves as a function of $2a$ ranging from 1 mm to 4 mm.

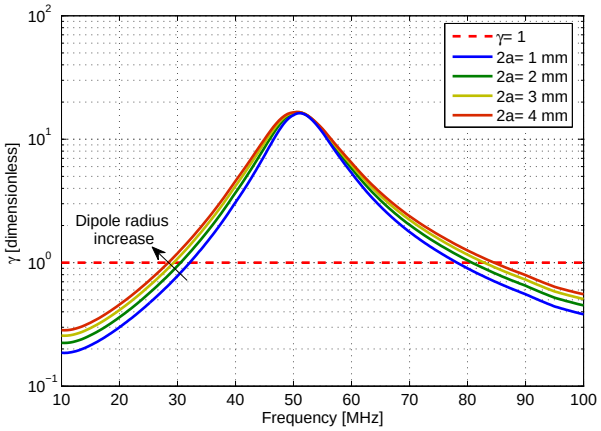

Fig. 15. Comparison of γ = 1 (dashed red line) with the calculated VSWR of the NEC-2 antenna simulation using a realistic ground plane as function of frequency for $2a$ ranging from 1 to 4 mm.

TABLE I
RELATION BETWEEN THE ANTENNA RADIATOR DIAMETER AND THE USEABLE FREQUENCY RANGE

$2a$ [mm]	$\nu(\gamma > 1)$ [MHz]	$\Delta\nu$ [MHz]
1	32.1 – 78.2	46.1
2	30.5 – 80.8	50.3
3	29.3 – 82.9	53.6
4	28.4 – 84.6	56.2

Comparing the simulation results shown in Fig. 15 with the result of the implemented antenna, see Fig. 3, some conclusions are evident: 1) increasing the diameter of the dipole conductor and keeping all other dimensions of the antenna shown in Fig. 3, the frequency bandwidth limited by galactic noise increases as well, 2) with increasing the diameter of the conductor a subtle reduction in resonant frequency (where γ presents the maximum value) is observed when increasing the diameter of the conductor, i.e., with a diameter of 1 mm, the maximum γ occurs at ∼51.5 MHz, increasing the diameter the maximum value of γ shifts to lower frequencies, reaching ∼50.5 MHz with a diameter of 4 mm, and 3) it is observed that a diameter increasing of 400% results in a galactic noise limited frequency bandwidth increase of about 21.9%, from the range of 32.1–78.2 MHz (with $2a$ = 1 mm) to 28.4–84.6 MHz (with $2a$ = 4 mm). Table I shows more details about the useable frequency range.

Despite of increasing in radiator wire diameter results in an increasing useful range of the antenna, aiming to have a low cost structures antenna we chose to keep the diameter wire as $2a$ = 1 mm.

From this point, the effects of varying the length of the

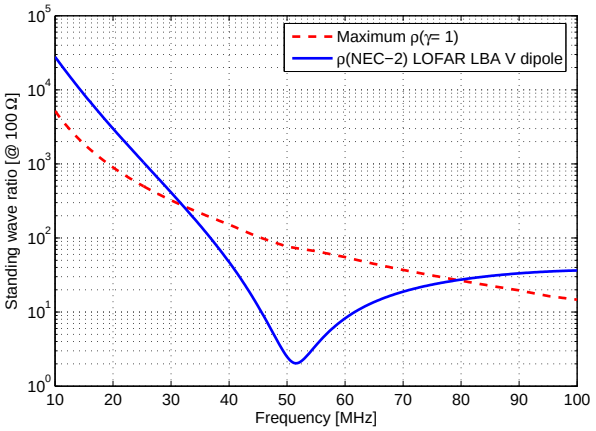

Fig. 16. Comparison between the NEC-2 simulated standing wave ratio for the antenna shown in Fig. 3 and the maximum allowed galactic noise limited ρ.

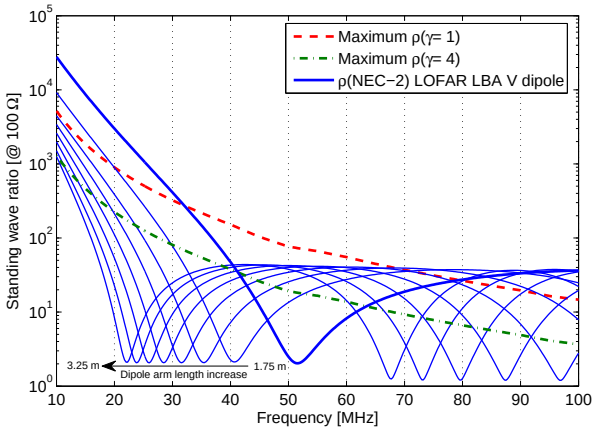

Fig. 17. Comparison between the NEC-2 simulated standing wave ratio for the antenna shown in Fig. 3 ranging ℓ parameter from 1.75 to 3.25 m and the maximum allowed galactic noise limited ρ (dashed-strong red line). The maximum allowed galactic noise 6.02 dB limited ρ is shown by the point-dashed green line.

dipole antenna ℓ will be verified. In this investigation, the dipole diameter is kept constant in all simulations, $2a$ = 1 mm.

Before further investigation, it is necessary to estimate the maximum allowable ρ where the antenna operate limited by galactic noise. Isolating ρ in (12), we have

$$\rho \approx 4e_r \frac{T_{sky}}{T_{pre}\gamma}. \tag{13}$$

The maximum allowable ρ is obtained when γ = 1. Using the Cane galactic noise model to calculate T_{sky}, and using the measured noise temperature of MAR-8 preamplifier (see Fig. 8), we get the maximum active antenna galactic noise limited ρ as a frequency function. Fig. 16 shows the curve of maximum ρ.

The curve of the simulated VSWR of the antenna shown in Fig. 3 is compared with the maximum admissible ρ. According to Fig. 16, it is clear the advantage of increasing the dipole arms length ℓ, i.e., the dipole V antenna resonance is shifted to lower frequencies. Thus, we take advantage of VSWR dipole V antenna curves and the curve of maximum permissible ρ, in order to obtain a higher bandwidth limited by the galactic noise.

Fig. 17 shows the simulation results of ρ varying the parameter ℓ from 1.75 to 3.25 m, with step of 25 cm. The influence of variation of h was not explored, and the value of the antenna mast height was increased just to keep the antenna wires above the ground plane, whereas in simulations the influence of varying h does not result in significant differences in the galactic noise limited frequency range.

From the simulations of the dipole V antenna is possible to build Table II, which relates the frequency range limited by galactic noise with the radiators length. The antenna mast height h is also listed.

The best dipole length configuration among those evaluated in Table II is for ℓ = 2.25 m, where the whole spectrum between 10 and 100 MHz is galactic noise limited. This antenna configuration presents the pattern shown in Fig. 18, that shows the antenna have very broad beamwidth and a small gain at and below the horizon, as was previously assumed to simplify (1) to (2). Fig. 17 also shows the maximum acceptable ρ for a difference of 6.02 dB (γ = 4) between the power due to T_{sky} and the instrumental noise. A large value of γ enables the integration time reduction to the minimum possible, and as assumed by [5], γ = 4 is assumed to be sufficient for this application. As shown in Fig. 17, the inverted V dipole antenna has a small portion of the spectrum limited by the galactic noise due to γ = 4. This motivates the search of other radiating structures that allow a greater frequency range galactic noise

TABLE II
RELATION BETWEEN THE ANTENNA RADIATOR LENGTH AND THE USEABLE FREQUENCY RANGE FOR DIPOLE V ANTENNA

ℓ [m]	h [m]	$\nu(\gamma > 1 \in [10.0, 100.0])$ [MHz]	$\Delta\nu$ [MHz]
1.75	1.6	19.9 – 71.0	51.1
2.00	1.6	10.0 – 68.4 ∪ 93.2 – 100.0	74.2
2.25	1.8	10.0 – 100.0	90.0
2.50	2.0	10.0 – 98.0	88.0
2.75	2.2	10.0 – 90.7	80.7
3.00	2.4	10.0 – 84.7	74.7
3.25	2.7	10.0 – 80.1	70.1

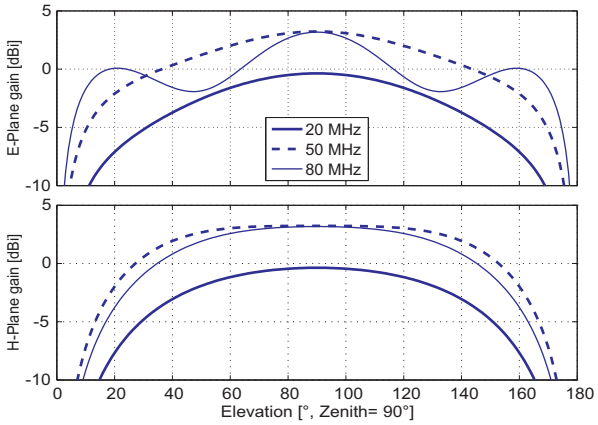

Fig. 18. Copolarized patterns at 20, 50 and 80 MHz for the best inverted V dipole arm length evaluated: ℓ = 2.25 m.

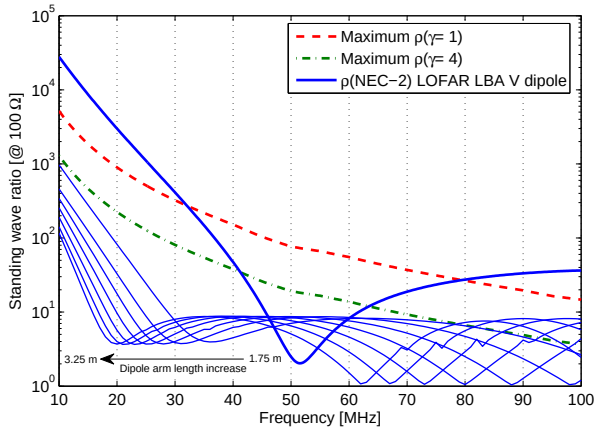

Fig. 20. Comparison between the NEC-2 simulated standing wave ratio for the antenna shown in Fig. 19 ranging ℓ parameter from 1.75 to 3.25 m and the maximum allowed galactic noise limited ρ (dashed-strong red line). The maximum allowed galactic noise 6.02 dB limited ρ is shown by the point-dashed green line.

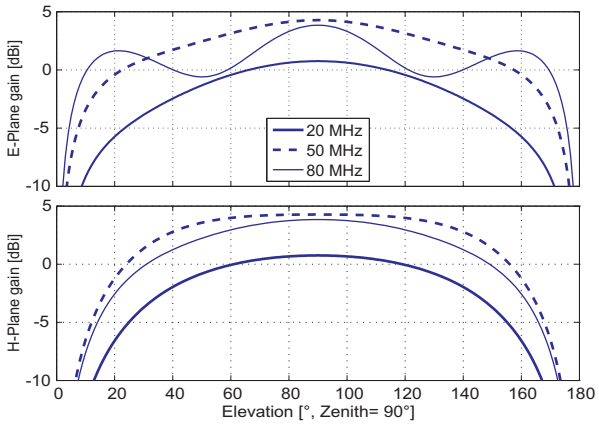

Fig. 21. Copolarized patterns at 20, 50 and 80 MHz for the best fork antenna arm length evaluated: ℓ = 2.00 m.

TABLE III
RELATION BETWEEN THE ANTENNA RADIATOR AND THE USEABLE FREQUENCY RANGE FOR FORK ANTENNA

ℓ [m]	h [m]	$\nu(\gamma > 4 \in [10.0, 100.0])$ [MHz]	$\Delta\nu$ [MHz]
1.75	1.6	10.0 – 100.0	90.0
2.00	1.6	10.0 – 100.0	90.0
2.25	1.8	10.0 – 97.4	87.4
2.50	2.0	10.0 – 92.2	82.2
2.75	2.2	10.0 – 86.5	76.5
3.00	2.4	10.0 – 81.6	71.6
3.25	2.7	10.0 – 78.6 ∪ 96.0 – 100.0	72.6

limited.

2) Fork Antenna: The fork antenna was investigated by [19] for the Long Wavelength Array (LWA) as a low cost alternative to replace the big blade antenna, used so far in LWA developing. The dimensions of the antenna fork are detailed in Fig. 19. The fork antenna proposed by [19] employs a dipole arm length of ℓ = 1.5 m and a mast height of h = 1.5 m.

The antenna was investigated using the same galactic noise model described previously, and using the same instrumentation. All the simulation of fork antenna employs diameter $2a$ = 1 mm, $\Psi = 90^\circ$ and $\Psi' = 15^\circ$. The main investigated parameter was the antenna arm length ℓ.

Fig. 20 shows the simulation results of ρ varying the parameter ℓ from 1.75 to 3.25 m for the fork antenna, with step of 25 cm. The influence of variation of h was not explored, and the value of the antenna mast height was increased just to keep the antenna wires above the ground plane.

Fig. 20 shows the maximum acceptable ρ for a galactic noise limited by 0 dB and 6.02 dB. The LOFAR LBA antenna γ is also shown. Here, it is evident the advantages of fork antenna compared to inverted V dipole antenna: all fork antennas are limited by the simulated galactic noise between 10 to 100 MHz for γ = 1, and for γ = 4 a large part of spectrum is usable.

From the simulations of fork antenna we present Table III, which relates the frequency range limited by galactic noise with the radiators length. The antenna mast height h is also listed. The best dipole length configuration among those evaluated in Table III is for ℓ = 2.00 m, where the whole spectrum between 10–100 MHz is galactic noise limited. For ℓ = 1.75 m the same band of spectrum (10–100 MHz) is also limited by the galactic noise. However, despite this antenna using lower wire length, the antenna with ℓ = 2.00 m is more suitable because it has lower VSWR values at higher frequency, as shown in Fig. 20. This antenna configuration presents the pattern shown in Fig. 21, and as it was expected, meets the previous assumptions.

3) Performance Comparison: The active antenna improvements allowed a substantial bandwidth increasing. Despite several references that propose antennas for low frequency radio astronomy, [2], [4], [7], [19], most of them show only practical results of measurements to suppose the galactic noise antenna useful frequency range. This method although more practical, cannot be true for all situations. The work of [5] presents a methodology similar to this paper, and employs the same galactic noise model: proposed by [11]. Thus, the comparison with the work of [5] seems more appropriate than a comparison with the other references.

The inverted V dipole antenna described in [5] is similar to V dipole described in the paper; however, it uses copper pipes radiators with ∼1/2 inch of diameter and the arm dimensions are smaller. Reference [5] has assessed two antennas assuming a preamplifier impedance of 200 Ω and 400 Ω, respectively to the NLTA and dipole V antennas. The active antenna proposed here has an input impedance of 100 Ω, that is given by two monolithic amplifiers MAR-8. Using commercial amplifiers, that has typical impedance of 50 Ω or 75 Ω, the results of [5] would only be feasible using an impedance transformation stage between the dipole radiator arms and the preamplifier input. The active antenna usable bandwidth can be increased by raising the preamplifier impedance, because, as shown in Fig. 23 and Fig. 17, the evaluated antennas have a high VSWR at periphery of resonant frequency, for a load impedance of 100 Ω (preamplifier) reaching values of 3×10^4 at 10 MHz for the dipole V. According to (10), the VSWR will be small for small values of reflection coefficient. In turn, the reflection coefficient, given by (5), will tend to smaller values when: 1)

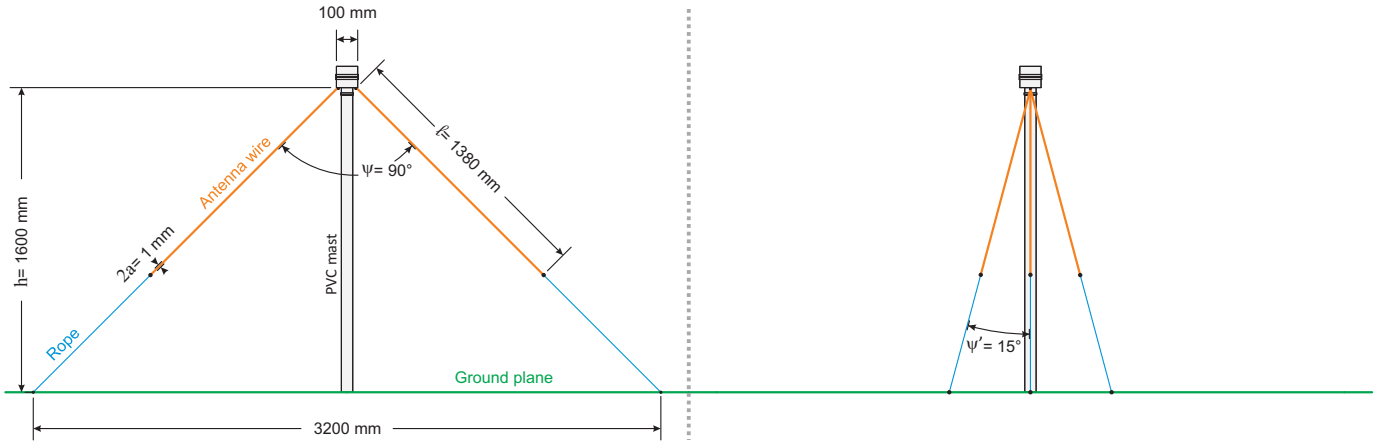

Fig. 19. Front view and side view of the fork antenna.

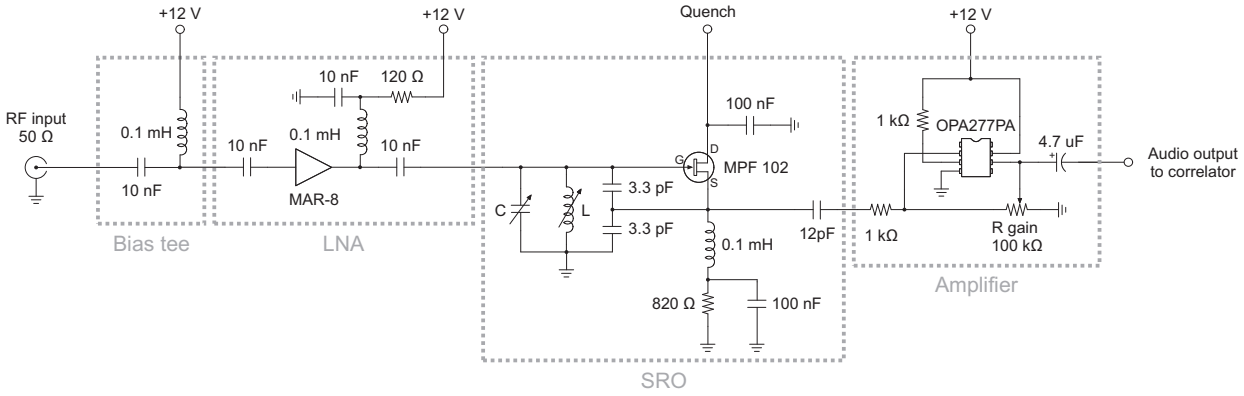

Fig. 22. Super-regenerative receiver circuit proposed.

TABLE IV
COMPARISON BETWEEN THE ACTIVE ANTENNA CHARACTERISTICS AND THE USEABLE FREQUENCY RANGE

Ref.	Antenna	Z_p [Ω]	T_{pre} [K]	$\nu(\gamma > 6$ dB) [MHz]	$\nu(\gamma > 10$ dB) [MHz]
[5]	NLTA	200	360	10 – 70	10 – 51
[5]	Dipole V (ℓ = 1.90 m)	400	360	19 – 66	33 – 46
This work	Dipole V (ℓ = 2.25 m)	100	220 – 252.5 (Fig. 8)	20 – 45 ∪ 92 – 100	24 – 39 ∪ 96 – 98
This work	Fork (ℓ = 2.00 m)	100	220 – 252.5 (Fig. 8)	10 – 100	10 – 48
This work	Fork (ℓ = 2.75 m)	100	220 – 252.5 (Fig. 8)	10 – 87	10 – 79

(Z_p + Z_a) $\rightarrow \infty$, and 2) when (Z_p – Z_a) $\rightarrow$ 0. Thus if Z_a presents high values along the spectrum, the increase of Z_p results in lower values of VSWR and consequently in higher values of γ (see (12)).

Another interesting point for comparisons is that the antennas of [5] ware assessed with copper pipes radiator with a diameter greater than 15 times the wire diameter used in this paper. In other words, large radiator diameters result in larger values of γ. The evaluation of radiator diameter was performed and the results of Fig. 15 showed that increasing the radiator diameter increases the useful bandwidth.

The conclusion is that employing a high preamplifier input impedance and a radiator diameter much high, the active antenna useful bandwidth will increase significantly. However, these changes involve significant costs. Table IV compares the spectrum galactic noise limited by 6 dB and 10 dB for fork and dipole V antennas. Fig. 23 shows the simulated standing wave ratio for the inverted V with ℓ = 2.25 m and fork with ℓ = 2.00 m. The value of γ for the fork antenna with ℓ = 2.75 m is also highlighted. From Table IV it is clear that NLTA and the fork antenna have compatible galactic noise limited bandwidth.

The antenna fork with ℓ = 2.75 m stands out because it can cover the range 10–79 MHz, almost the entire spectrum of the interferometer interest (20–80 MHz) with a difference of 10 dB between the galactic noise and the instrumental noise. However, it is interesting employment compact antennas, and it is assumed that a signal (galactic noise) 6 dB higher than the instrumental noise is enough for operability. Thus, despite fork antenna with ℓ = 2.75 m perform better, to reduce the size of antennas, fork with ℓ = 2.00 m still the best choice. The antennas proposed in the paper seem cheaper than those proposed by [5]. The reason is the cost of an additional impedances transformer (to obtain Z_p = 200 Ω or 400 Ω) and

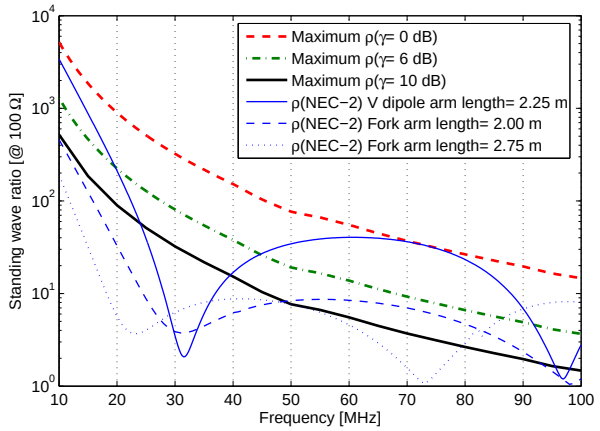

Fig. 23. Comparison between the NEC-2 simulated standing wave ratio for the inverted V dipole and Fork antennas with the maximum allowed galactic noise ρ limited by 0, 6 and 10 dB.

the costs of copper pipes, that is more expensive than simple wires. The performance antennas proposed here is as good or better than the [5] antennas.

B. Reviewing the Receiver

In order to minimize the receiver frequency offset and to fix problems of isolation between the receiver and active antenna the super-regenerative receiver circuit is proposed in Fig. 22. The main differences between the receiver implemented (Fig. 13) and the proposed (Fig. 22) is the employment of an external quench oscillator, and the lower number of active components. A super-regenerative receiver with external quench was implemented with the following blocks: 1) a bias tee, 2) a low noise amplifier (LNA), 3) a super-regenerative oscillator (SRO), and 4) a low frequency amplifier.

The LNA is often included to minimize the radiation return from SRO to antenna. Thus, in addition to providing a high gain, the LNA also provides the signal isolation between the RF antenna and the SRO, and even radiation from the SRO and itself. Another positive point added to the LNA is that the noise figure of the receiver will be dominated by the LNA.

The SRO active element is a MPF 102 JFET transistor, whose current is given by the source bias resistor. The polarization of the JFET is performed when the quench oscillation has positive voltage values. The central frequency is given by the values of the inductor L and the equivalent capacitance of series capacitor of 3.3 pF in parallel with the capacitor C.

C. Cost Analysis

Here we aim to make evident the low cost condition of the implemented interferometer by detailing the costs for the active antenna and receivers. Tables V, VI and VII present the component name, the component quantity, the cost referent to the assigned quantity and the vendor name. The cost of each electronic component is expressed in United States of America currency and was obtained from the vendors Digi-Key (http://www.digikey.com) or Mini-Circuits (https://www.minicircuits.com). Table V presents the costs for

TABLE V
BILL OF MATERIALS – ACTIVE ANTENNA

Part	Quantity	Cost [US$]	Vendor
Monolithic amplifier	2	2.64	Mini–Circuits
Ceramic capacitor (10 nF)	8	0.8	Digi-Key
RF chock inductor (0.1 mH)	3	0.5514	Digi-Key
Resistor (100 Ω)	2	0.28	Digi-Key
BNC male connector (50 Ω)	1	1.544	Digi-Key
Balun	1	3.9	Mini–Circuits
Diode	1	0.14	Digi-Key
Copper wire – 1 mm	4 (meters)		
PCB board	1		
PVC antenna mast	1		
	Total	9.8554	

TABLE VI
BILL OF MATERIALS – RECEIVER BASED ON MK484

Part	Quantity	Cost [US$]	Vendor
BNC male connector (50 Ω)	1	1.544	Digi-Key
P2 female connector	1	0.519	Digi-Key
RF chock inductor (0,1 mH)[1]	1	0.1838	Digi-Key
RF ceramic Capacitor (10 nF)[1]	1	0.1	Digi-Key
Broband inductors[2]	4		
Ceramic capacitor (67 pF)[2]	1	0.096	Digi-Key
Ceramic capacitor (76 pF)[2]	2	0.1	Digi-Key
Ceramic capacitor (83 pF)[2]	1	0.105	Digi-Key
Ceramic capacitor (101 pF)[2]	1	0.075	Digi-Key
Ceramic capacitor (100 nF)	4	0.048	Digi-Key
Electrolytic capacitor (100 nF)	1	0.1004	Digi-Key
Inductor – tank circuit	1		
Isolation transformer 1:1[3]	1		
Variable capacitor (3–20 pF)[3]	1	1.513	Digi-Key
Resistor (1 kΩ)	5	0.129	Digi-Key
Resistor (2.2 kΩ)	1	0.129	Digi-Key
Resistor (3 kΩ)	2	0.399	Digi-Key
Resistor (9.09 kΩ)	1	0.399	Digi-Key
Resistor (10 kΩ)	1	0.399	Digi-Key
Resistor (100 kΩ)	1	0.399	Digi-Key
Resistor (560 kΩ)	1	0.399	Digi-Key
OPA277PA audio amplifier	1	2.142	Digi-Key
Variable resistor (10 kΩ)	1	0.496	Digi-Key
LED (3 mm)	1	0.334	Digi-Key
BC458 transistor	3	0.792	Digi-Key
PCB board	1		
	Total	11.4162	

[1]Bias tee. [2]Impedance matching. [3]Tank circuit.

the active antenna circuit. The costs presented in Tables VI and VII are related to the receivers illustrated in Fig. 13 and 22, respectively. The total costs for the active antenna and the receivers (presented in Fig. 13 and Fig. 22) are, respectively: US$ 9.90; US$ 11.40; and US$ 11.60. In order to have a reference parameter, it was studied the LOFAR article [20], which mentions a value of US$ 21,000.00 considering the 96 LBA antennas of a LOFAR station, it means approximately, US$ 219.00 for one antenna and one receiver.

IV. CONCLUSIONS

The proposed system can operate satisfactorily in the range of 32–78 MHz using a LOFAR LBA inverted V-shape dipole radiator. The modifications described in this paper allow the radiator to increase the frequency range galactic noise limited to the whole spectrum between 10 and 100 MHz. The evaluation of other kinds of low cost antennas allowed improvements in the fork antenna, allowing the interferometer

TABLE VII
BILL OF MATERIALS – RECEIVER ILLUSTRATED ON FIG. 22

Part	Quantity	Cost [US$]	Vendor
BNC male connector (50 Ω)	1	1.544	Digi-Key
P2 female connector	1	0.519	Digi-Key
Ceramic capacitor (10 nF)	4	0.4	Digi-Key
Ceramic capacitor (100 nF)	2	0.748	Digi-Key
Ceramic capacitor (0.3 pF)	2	0.048	Digi-Key
Ceramic capacitor (12 pF)	1		
RF chock inductor RF (0,1 mH)[1]	1	0.1838	Digi-Key
Monolithic amplifier	1	1.32	Mini–Circuits
BF245C JFET transistor	1	0.371	Digi-Key
Electrolytic capacitor (4.7 μF)	1	0.3938	Digi-Key
OPA277PA audio amplifier	1	2.142	Digi-Key
Resistor (120 Ω)	5	0.129	Digi-Key
Resistor (820 Ω)	1	0.33	Digi-Key
Resistor (1 kΩ)	2	0.258	Digi-Key
Variable resistor (100 kΩ)	1	0.496	Digi-Key
Variable capacitor (3–20 pF)[2]	1	1.513	Digi-Key
Ferrite variable inductor (220 nH)	1	1.2	Digi-Key
Quench generator	1		
PCB board	1		
	Total	11.60878	

[1]Bias tee of SRO. [2]Tank circuit.

to operate about 6 dB galactic noise limited. Another important fact was the design of an extremely low cost RF receiver for the LOFAR LBA range.

ACKNOWLEDGMENT

This work was supported in part by National Council of Scientific and Technological Development of Brazil (CNPq). The authors also acknowledge the Program PIBIC/INPE - CNPq/MCT – Brazil for fellowship.

REFERENCES

[1] J. D. Bregman, "Concept design for a low-frequency array," in *Society of Photo-Optical Instrumentation Engineers (SPIE) Conference Series*, 2000.
[2] G. H. Tan and C. H. Rohner, "Low-frequency array active-antenna system," in *Society of Photo-Optical Instrumentation Engineers (SPIE) Conference Series*, 2000.
[3] H. Falcke *et al.*, "Detection and imaging of atmospheric radio flashes from cosmic ray air showers," *Nature*, vol. 435, pp. 313–316, May 2005.
[4] S. Ellingson, J. Simonetti, and C. Patterson, "Design and evaluation of an active antenna for a 29–47 MHz radio telescope array," *IEEE Trans. Antennas Propag.*, vol. 55, no. 3, pp. 826–831, Mar. 2007.
[5] S. Ellingson, "Antennas for the next generation of low-frequency radio telescopes," *IEEE Trans. Antennas Propag.*, vol. 53, no. 8, pp. 2480–2489, Aug. 2005.
[6] F. X. Moncunill-Geniz *et al.*, "An 11-mb/s 2.1-mw synchronous super-regenerative receiver at 2.4 ghz," *IEEE Trans. Microw. Theory Tech.*, vol. 55, no. 6, pp. 1355–1362, Jun. 2007.
[7] K. Stewart *et al.*, "Lofar antenna development and initial observations of solar bursts," *Planetary and Space Science*, vol. 52, no. 15, pp. 1351–1355, 2004. [Online]. Available: http://www.sciencedirect.com/science/article/B6V6T-4DS7T4M-1/2/27e2ecf1a3b30d08daa23d9055a309f3
[8] "MAR-8 data sheet," Mini-Circuits, New York, U.S.A.
[9] W. A. van Cappellen, M. Ruiter, and G. W. Kant, "Low band antenna: Architectural design document," ASTRON, Tech. Rep. LOFAR-ASTRON-ADD-009, Mar. 2007.
[10] J. Jones, "Analysis of the symmetric center-fed v-dipole antenna," *IEEE Trans. Antennas Propag.*, vol. 24, no. 3, pp. 316–322, May 1976.
[11] H. V. Cane, "Spectra of the non-thermal radio radiation from the galactic polar regions," *Monthly Notices of the Royal Astronomical Society*, vol. 189, pp. 465–478, Nov. 1979.
[12] International Telecommunications Union, "Radio noise," ITU-R Rec. P.372-8, Apr. 2003.
[13] A. Horneffer *et al.*, "LOPES: detecting radio emission from cosmic ray air showers," in *Society of Photo-Optical Instrumentation Engineers (SPIE) Conference Series*, 2004.
[14] J. D. Kraus, *Radio Astronomy*, 2nd ed. Powell, Ohio, USA: Cygnus-Quasar, 1972.
[15] C. Bowick, *RF Circuit Designs*. Indianapolis, IN, USA: Howard W. Sams & Co. Inc, 1982.
[16] T. R. Cuthbert Jr., *Broadband Direct-Coupled and Matching RF Networks*. Greenwood, AR, USA: TRCPEP, 1999.
[17] "MK484 data sheet," Rectron Semiconductor, Chino, California, USA.
[18] "BC548 data sheet," Fairchild Semiconductor, San Jose, California, USA.
[19] N. Paravastu, B. Hicks, P. Ray, and W. Erickson, "A candidate active antenna design for a low frequency radio telescope array," in *Antennas and Propagation Society International Symposium, 2007 IEEE*, Jun. 2007, pp. 4493–4496.
[20] T. Feder, "Tiny antennas form vast radio telescope array," *Physics Today*, vol. 64, no. 24, pp. 24–26, Mar. 2011.

Guilherme S. Rosa received his B.S. degree in Electrical Engineering from Federal University of Santa Maria in 2011. He is currently working toward his M.Sc. degree in Applied Electromagnetics at the Catholic University of Rio de Janeiro.

Nelson J. Schuch is graduated in Physics by The Federal University of Santa Maria - UFSM, Brazil. Master of Science in Astrophysics by The Mackenzie University, Brazil. Ph.D. and Post Doctor in Physics - Astrophysics by The University of Cambridge, England. Mentor of the actions for the development and construction of the INPE's Southern Regional Space Research Center and The Southern Space Observatory in The South of Brazil, at Santa Maria, RS. Currently Senior Researcher at INPE/MCTI, Santa Maria, Brazil.

Natanael R. Gomes received the Electrical Engineering degree from Federal University of Santa Maria in 1993, Master of Science and Doctoral degrees in Electrical Engineering with emphasis in Telecommunications and Telematics from State University of Campinas in 1996 and 2000, respectively. In October 2000, he joined the Ericsson Company in Indaiatuba, São Paulo, Brazil, where he worked in research and development on Mobile Telephony - CDMA until February 2002. In March 2002 he joined as professor at the University Vale do Rio Doce - UNIVALE in the city of Governador Valadares, Minas Gerais, Brazil, where he was coordinator of the Electrical Engineering/Telecommunications course. He is currently a professor at Electronic and Computer Department and coordinator of the Electrical Engineering Course in Federal University of Santa Maria, Brazil. Also, he is a researcher at The Santa Maria Space Science Laboratory - LACESM/CT-UFSM and a member of the signal Processing and Communication Group - GPSCom - UFSM. He has experience in Electrical Engineering with emphasis on Telecommunications, acting on the following topics: Pattern Recognition, Signal Processing, Antennas and Wireless Communication.

J. R. Bergmann (M'89) received the degree of electrical engineer from Universidade Federal do Rio Grande do Sul, Brazil, in 1975, the M.Sc. degree in electrical engineering from Instituto Militar de Engenharia, Brazil, in 1979, and the Ph.D. degree in electrical engineering from Queen Mary College, University of London, London, U.K., in 1986.

He is an Associate Professor at the Catholic University of Rio de Janeiro, Rio de Janeiro, Brazil, where he is also the Head of the Antenna Group of the Center of the Telecommunications Studies (CETUC). Since 2007, he is also Vice President for Academic Affairs of the Catholic University of Rio de Janeiro. His research interests comprise numerical modeling, synthesis and analysis of reflector systems. Dr. Bergmann was Vice President and President of the Brazilian Microwave and Optoelectronics Society (SBMO) from 1996 to 2000.

Ezequiel Echer is Doctor in Space Geophysics (2003) by INPE, and is currently a researcher of the Space Geophysics Division of INPE. He has developed PhD Thesis in the study of the geomagnetic effects of solar wind interplanetary structures. He accomplished pos-doctorate (2005) in the Max Planck Institute of Solar System Research, Germany, studying the answer of the terrestrial magnetosphere to the solar wind disturbances with the Cluster constellation. Nowadays he studies the solar wind-planetary magnetospheres coupling, interplanetary MHD shocks, discontinuities and waves properties in the heliosphere.

Renato Machado (S´04-M´08) received the B.S.E.E. degree from the São Paulo State University (UNESP), Ilha Solteira, SP, Brazil, in 2001. He received the M.Sc. degree and the Ph.D. degree in electrical engineering from the Federal University of Santa Catarina (UFSC), Florianópolis, SC, Brazil, in 2004 and 2008, respectively. He was a visiting researcher in the Department of Electrical Engineering, Arizona State University (ASU), Tempe, AZ, U.S.A., from August 2006 to June 2007. He was a research engineer at Nokia Institute of Technology, Brazil, from October 2007 to March 2008, and a visiting Professor in the Department of Electrical Engineering, Federal University of Juiz de Fora, MG, Brazil, from September 2008 to August 2009. Since August 2009 he has been a Professor in the Federal University of Santa Maria, RS, Brazil. His research interests include MIMO systems, space-time coding, cooperative communication, wireless communications, and power line communications.

Dr. Machado is a member of the IEEE Communications Society, and the Brazilian Telecommunications Society.